Adsorption of End-Functionalized Polystyrene on Model Textured Surfaces

N. Singh, A. Karim,† F. S. Bates, and M. Tirrell*

Department of Chemical Engineering and Materials Science, University of Minnesota, Minneapolis, Minnesota 55455

K. Furusawa

Department of Chemistry, University of Tsukuba, Tsukuba, Ibaraki 305, Japan

Received May 6, 1993; Revised Manuscript Received December 30, 1993®

ABSTRACT: Adsorption of iminium ion end-functionalized polystyrene on model rough surfaces has been investigated. The model surfaces were prepared by spin coating a solution of colloidal silica beads on aluminum-coated silicon surfaces. Atomic force microscopy and scanning electron microscopy of the surfaces revealed a nearly hexagonal packing of beads. Static secondary ion mass spectroscopy and X-ray photoelectron spectroscopy have been used to measure relative changes in the adsorbed amounts on the model surfaces compared to a flat surface. We observe a significant enhancement of adsorption when the bead to polymer radius (ρ/R_g) is of order unity. For $\rho/R_g \gg 1$, the adsorbed amounts approach that on the smooth surfaces, whereas for $\rho/R_g < 1$, the adsorption is substantially reduced. The enhancement in adsorption is interpreted as a favorable reduction in crowding or stretching energy on adsorption, whereas the reduction is understood in terms of topologically induced steric hindrance to adsorption.

Introduction

Polymer adsorption finds extensive applications in modifying physical and chemical properties of surfaces. For instance, block copolymers and end-functionalized polymers can be tethered[1] to a surface by virtue of a "sticky" group which anchors to the solid surface while the rest of the chain remains solvated and nonadsorbed. This alters the interfacial properties[2,3] to that of the overlaying polymer layer and finds applications in colloidal stabilization, improved biocompatibility of surfaces for biomedical applications, enhanced wetting and adhesion properties of surfaces, and numerous other applications.

Grafting of polymers on flat, smooth surfaces has received considerable theoretical[4–9] and experimental[10–14] attention. Equilibrium grafting density via end adsorption is a balance between the enthalpic gain in free energy due to the bonding of the chain end to the surface and the increased stretching energy due to overlap of the chains as the grafting density increases. The total amount of polymer adsorbed is governed by the strength of the polymer–surface interaction, solvent quality, and the molecular weight of the polymer. The influence of surface curvature on adsorption and end anchoring has been theoretically[15–26] and experimentally[27–29] investigated. All these studies have, however, considered the case of smooth surfaces for theoretical and experimental convenience.

In this paper, we aim to begin experimentally to illuminate effects of surface texture on polymer adsorption and grafting. We use the generic term "rough" to describe, in a crude fashion, the characteristics of "texture". In fact, in this paper we explore but one specific texture. We do not answer all questions of how surface topography can affect surface binding of polymers. However, we demonstrate two significant effects with broad applicability to polymer binding on rough surfaces.

In a seminal paper, Hone[30] et al. studied theoretically the influence of sinusoidal surface fluctuations on homopolymer adsorption. This was followed by a series of theoretical investigations by Blunt[31] et al., Ligoure and Leibler,[32] Balazs[33] et al., and Andelman and Joanny.[34] Their work has highlighted the effect of surface roughness at the size scale of the adsorbing polymers on the total amount of polymer adsorbed. The influence of roughness on adsorption has, however, not received experimental attention. Most experimental studies have used mica, polished silicon wafers, and metals as substrates for these studies. The convenience of smoothness provides ideality to the study without introducing the complexities due to the randomness of the surface fluctuations. A systematic experimental effort to complement the theoretical work on the role of roughness has been lacking.

To understand the influence of surface curvature on polymer adsorption, we have synthesized model rough surfaces where some of the these theoretical predictions can be systematically tested. These surfaces were synthesized by spin coating a solution of colloidal silica beads on Al-coated Si surfaces. Such surfaces then provide a template wherein the surface roughness defined by the bead size can be controlled by changing the size of the silica spheres during their chemical synthesis.

Adsorption of end-functionalized polymers on *isolated* cylindrical and spherical bumps on a flat surface has been theoretically addressed by Ligoure and Leibler.[32] Spherical and cylindrical surfaces favor adsorption due to the reduction in the stretching energy with curvature for fixed grafting density of the polymer. In terms of the blob model[15] illustrated in Figure 1, the reduction in stretching energy results from an increase in blob size with distance from the surface. This increase in blob size implies more volume available per chain for the same surface density and results in a chain length (L) for spherical ($L \sim N^{3/5}$) and cylindrical ($L \sim N^{3/4}$) surfaces reduced as compared to flat surfaces ($L \sim N$) for densely end-adsorbed polymers.[1] At equilibrium, the chemical potential of the adsorbed chains has three main components, which are the free energy (Δ) gain due to the end group sticking to the surface, loss of translational entropy ($\ln \sigma$) of chains in the adsorbed layer, and the average chain deformation and excluded volume free energy ($f_d(\sigma)$) different from that of the free chain due to the interactions imposed by

† Current address: National Institute of Standards and Technology, Gaithersburg, MD 20899.

® Abstract published in *Advance ACS Abstracts*, March 1, 1994.

0024-9297/94/2227-2586$04.50/0

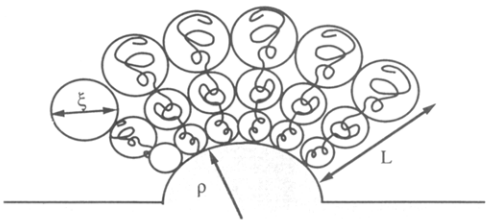

Figure 1. Adsorption of end-functionalized PS on one single spherical bump on a flat surface. ρ is the radius of the bump and L is the stretched chain length. The blob size ξ increases as a function of distance from the bump.

grafting. The chemical potential[32] of the grafted chains in solution can then be written as

$$\mu_{ext} = \mu_d(\sigma) = kT[-\Delta + \ln \sigma + f_d(\sigma)] \quad (1)$$

where μ_{ext}, the chemical potential of chains in solution in contact with the surface, is equal to that of the chains adsorbed on the surface ($\mu(\sigma)$), with σ being the surface coverage. Using this expression for the chemical potential and varying blob size as a function of distance from the surface for the different geometric models,[15] Ligoure and Leibler[32] predict increasing surface coverage with dimensionality d, i.e., spherical > cylindrical > flat. They also predict an enhancement of grafting density when the radius of curvature is smaller than the thickness of the grafted layer on the flat portions of the surface. Adsorption in valleys is expected to have a slightly lower surface density but close to that of the flat surface as there is no reason for the chains to conform to the surface if it results in an energy penalty.[32]

In this paper, we present results on adsorption of iminium ion end-functionalized polystyrene on model rough surfaces, studied as a function of bead size (40–6000 Å) and PS molecular weights (5700, 125000, and 285000). Static secondary ion mass spectroscopy (SIMS) and X-ray photoelectron spectroscopy (XPS) were used as the primary tools of investigation. The PS(91) peak from SIMS and the integrated carbon (C_{1s}) signal from XPS, both normalized by the substrate (Al) signal, provide a measure of the extent of adsorption. These ratios are further normalized by the smooth surface values to determine the relative increase or decrease in the surface density.

The methodology for the synthesis of these surfaces is presented first, followed by a description of surface characterization by ellipsometry, scanning electron microscopy (SEM), atomic force microscopy (AFM), and X-ray reflectivity. These different techniques establish packing, uniformity, and reproducibility of the model surfaces. Next, instrumentation and data analysis for XPS and SIMS is discussed, followed by results and comparison with theoretical predictions.

Experimental Section

Synthesis and Characterization of Model Surfaces. Model rough surfaces were prepared by spin coating a solution of colloidal silica beads on aluminum-coated polished silicon wafers. The colloidal solutions were chemically synthesized using the method developed by Stöber[35] et al. and Bogush[36] et al., which essentially involves hydrolyzing tetraethyl orthosilicate (TEOS) in 200 proof ethanol using ammonia as a catalyst. Relatively monodisperse colloidal solutions with particle sizes in the range 0.05–2 μm can be synthesized by varying the concentration of the various species. Particle size was characterized by scanning electron microscopy (SEM). In the limit of very small and very large bead sizes the surface approaches a smooth surface. Bead size can therefore be changed to effect a transition from a rough surface to a flat surface at either extreme of bead size. The various steps in the synthesis of these surfaces are schematically illustrated in Figure 2. The first step involves coating a thick layer (~1500–3000 Å) of Al (99.9% purity) on a polished Si wafer. The pressure in the evaporation chamber was 10^{-5} Torr, and Al was deposited at a rate of 5 Å/s. A solution of ~3 wt % colloidal silica in ethanol was then spin coated at a speed of ~2000 rpm. The choice of speed and solution concentration is critical in getting a close packing of the beads in a uniform monolayer. Lower speeds at the same concentration result in multilayers, and higher speeds result in uncovered areas on the surface. Close packing of the silica beads on the substrates was confirmed through SEM and AFM. Uniformity at various spots on the sample was checked through the invariance of ellipsometric parameters tan ψ and cos δ. Specular X-ray reflectivity from surfaces synthesized from the same solutions under similar conditions was identical, establishing reproducibility of the synthesis technique. Figure 3 is an atomic force micrograph of such a surface formed from the ~800-Å bead size colloidal solution. Aluminum was used as the base substrate as it was observed that these colloidal solutions formed more uniform films on aluminum as compared to polished silicon surfaces. The surfaces were further coated with a thin layer of Al (~40 Å) to immobilize the beads and enable the use of the Al signal as a reference signal for quantifying the SIMS data.

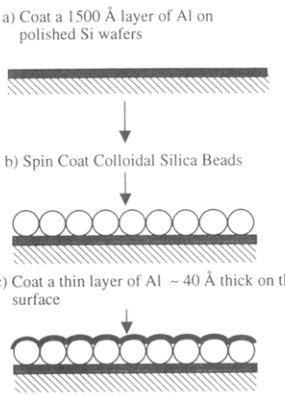

Figure 2. Synthesis of the model rough surfaces involves (a) coating a polished Si wafer with a ~1500-Å-thick layer of aluminum, (b) spin coating a solution of silica beads on the Al surface, and (c) coating the surface with a thin layer of Al ~ 40 Å.

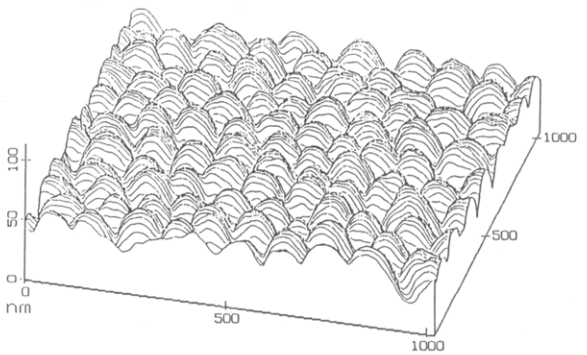

Figure 3. Atomic force micrograph of a model surface synthesized from the 800-Å-diameter silica beads. The image was obtained using a 200-μm-thick Si_3N_4 tip with a spring constant of 0.12 N/m. The scan rate was 8.7 Hz, and the nominal operating force was 3 nN.

Sample Preparation. Iminium end-functionalized polystyrene was synthesized by Furusawa[37] et al. using anionic polymerization followed by chemical modification with *N*-methyl-2-pyrrolidine (NMP) and then quenching with methanol. The chemistry of the synthesis is illustrated in Figure 4. Three molecular weights, 5700, 125000, and 285000, were used for the adsorption studies. Glass-distilled SPEC-grade toluene (EM Science) was used as received.

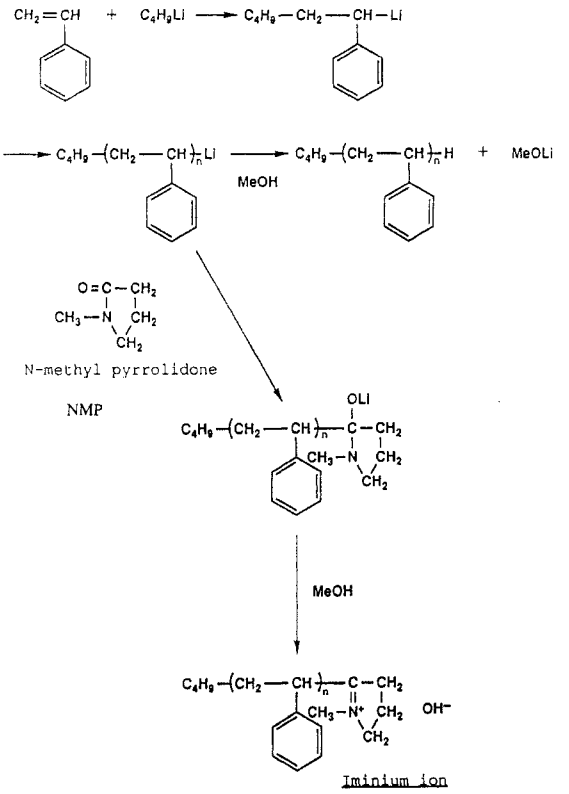

Figure 4. Chemistry of the synthesis of the end-functionalized PS used for the adsorption studies.

Ground-glass containers (ca. 1.5 cm × 6 cm) used for the adsorption experiments were cleaned overnight in nitric acid and then rinsed with ethanol. Next, these bottles were baked in a high-temperature kiln at ~550 °C to ensure removal of all carbonaceous contaminants and then rinsed in toluene. A nominal concentration of ~600 μg/mL of the polymer was used to prepare mother solutions, which were stored in ground-glass containers at room temperature for several days. Other bottles used for the adsorption studies were incubated with dilute polymer solutions to coat the walls of the container with the polymer and then rinsed with toluene. Prior to adsorption, the wafers were ozone cleaned under a UV lamp for 10 min followed by immediate rinsing with toluene. These wafers were immersed in the polymer solutions for 3–4 days to eliminate any temporal effects. Following the adsorption period, the wafers were rinsed in pure toluene and dried with nitrogen. The samples were then immediately taken for spectroscopic measurements.

Techniques. X-ray Photoelectron Spectroscopy. X-ray photoelectron spectroscopy data were acquired using a Perkin-Elmer Model 5400 spectrometer fitted with a nonmonochromatized Mg Kα X-ray source. The resolution of the spectrometer was set to 35.8-eV pass energy, and the source operated at 300 W. Under these conditions Parsonage[13] et al. had observed negligible damage to the polymers in a similar adsorption study of PVP–PS diblock copolymers. Total integrated intensities of the Si_{2p}, C_{1s}, O_{2p}, and Al_{2p} signals were obtained at vector takeoff angles ranging from 90° (normal) to 10° (grazing). The angle-resolved data were used to calculate the adsorbed amounts on a smooth surface. The ratio of the integrated carbon (C_{1s}) to the substrate Al_{2p} signal was used to estimate the relative enhancement or decrease in adsorption on the rough surface compared to that on the smooth surface. From such an analysis, it is not possible to extract absolute adsorbed amounts; however, it provides a convenient and quantitative indicator of the relative increase or decrease in adsorption.

Attenuation in the substrate signal from angle-resolved XPS cannot be used directly to compute the absolute amounts of polymer adsorbed on the rough surface, as the path traveled by the excited electrons varies with the surface topography. We have therefore used the normalized carbon signal as a direct measure of the extent of adsorption. The integrated carbon (C_{1s}) signal has been normalized with respect to the substrate Al_{2p} signal to provide a measure of the adsorbed amount. This ratio can be then compared to the smooth surface value to determine the relative increase or decrease in adsorption. R_{XPS} can be defined as

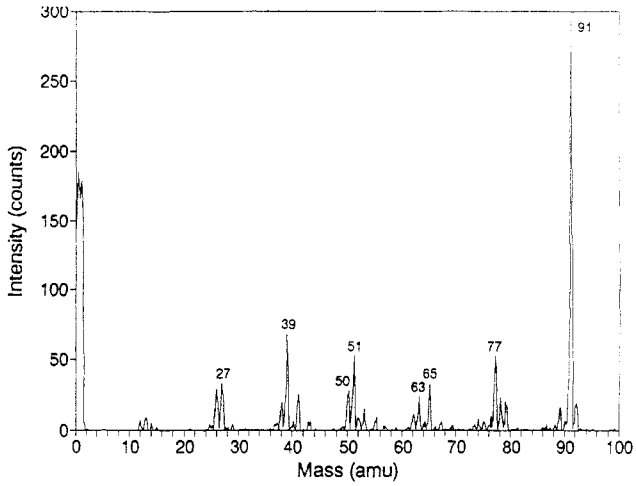

Figure 5. Characteristic polystyrene secondary ion mass spectrum. The strong PS(91) peak has been used as a measure of the presence of the polymer. The intensity of the PS(91) peak is divided by the substrate $Al^+(27)$ and $AlH^+(28)$ peaks to measure the extent of adsorption. This ratio is normalized with respect to the smooth surface values to determine the relative increase or decrease with respect to the flat surface.

$$R_{XPS} = \frac{[I(C_{1s})/I(Al_{2p})]_r}{[I(C_{1s})/I(Al_{2p})]_s} \quad (2)$$

where I is the intensity of the respective excited electrons. XPS has not been used as the primary tool of investigation for studying the rough surfaces. Instead, it has been mainly used to verify the consistency with the results from static SIMS as described below.

Secondary Ion Mass Spectroscopy. Quadrupole-based static secondary ion mass spectroscopy (SIMS)[38,39] was done at Evans Central, Minneapolis. The positive and negative secondary ion spectra were collected using a 0.15-nA, 7-keV Xe^+ primary beam rastered over a 1.5 × 1.5 mm^2 area. Under these conditions typical penetration depths expected for these systems is between 10 and 30 Å.[40] Measurements were made at a takeoff angle of 60° for incident angles normal to the surface. A typical pure PS positive secondary ion spectrum is shown in Figure 5. This spectrum was acquired from a thick polystyrene film spun cast from toluene on a polished Si wafer. Since the PS(91) peak corresponding to the $C_7H_7^+$ secondary ions is the strongest in the positive spectrum, this peak was used as a measure of the amount of polymer adsorbed on the surface.

Newman and Viswanathan[41] have demonstrated the linear relationship between the intensity of the molecular fragments in static SIMS and film thickness. In their study of perfluoropolyethers on carbon-coated Ni-containing hard disks, they have shown that the characteristic CF_3^+ signal varies linearly with film thickness up to ~30 Å. The film thickness was measured using ellipsometry and FTIR. Furthermore, they have also seen an increase in the intensity of the hydrocarbon peaks originating from the carbon layer below the lubricant as the film thickness decreases. After 30 Å saturation occurs. The saturation could be due to the film thickness exceeding the penetration depth in the case of homogeneous coverage, or if the film is noncontinuous, the saturation might occur when the film begins to completely cover the substrate. When the coverage is nonuniform, the average film thickness over the sampling area is measured. As a further test they have verified the applicability of this technique to other systems. A similar dependence has been observed for a long-chain ethoxylated alcohol surfactant film also. Prior calibration of the instrument is definitely required for quantifying the film thickness using static SIMS.

We have used XPS to quantify the adsorbed amounts on smooth surfaces[13] as explained below. Calibration of the fragment

Table 1

PS MW	τ/λ	τ (Å)	$s(\rho=1.03)$ (mg/m^{-2})	$\sigma \times 10^{-16}$ (m^{-2})	$\sigma_{ol} \times 10^{-16}$ (m^{-2})	σ/σ_{ol}
5700	0.5606	8.41	0.866	9.146	7.82	1.17
125000	0.6198	9.29	0.956	0.460	0.198	2.32
285000	0.5404	8.11	0.835	0.176	0.0746	2.35

signal from the polymer adsorbed on the rough surface is nontrivial as it is very difficult to measure the film thickness or the adsorbed amount directly. One possibility is to adsorb tritium-labeled polymer and then measure the adsorbed polymer using scintillation counting.[13] Since the aim of this work is to present the qualititative influence of surface texture on polymer adsorption, an extensive calibration of the signal from the rough surface was not attempted. The ratio of the PS(91) peak to the substrate signal was used as a measure of the adsorbed amount. Such an analysis is applicable when the penetration depth (~30 Å) exceeds the film thickness (~10 Å). The substrate signal in this case results from the $Al^+(27)$ ions and some contributions from the $AlH^+(28)$ peak. The pure PS spectrum also has a peak at the 27 amu position from the $C_2H_3^+$ ion, which was subtracted when calculating the net substrate signal. The ratio of the PS-(91) peak intensity to that of the sum of the $Al^+(27)$ and AlH^+-(28) peak intensities then gives a measure of the amount of polymer adsorbed. R_{SIMS}, a ratio similar to R_{XPS}, can be defined as

$$R_{SIMS} = \frac{[I(PS(91))/I(Al^+(27)) + I(AlH^+(28))]_r}{[I(PS(91))/I(Al^+(27)) + I(AlH^+(28))]_s} \quad (3)$$

In the two limits where the bead size goes to zero and infinity, these ratios (R_{SIMS} and R_{XPS}) would be expected to go to one as the beads approach the limit of zero and infinite curvature (smooth), thereby creating smooth surfaces in both limits.

This ratio measures the relative increase or decrease in adsorption. The measured enhancement or reduction in adsorption thus determined for the model rough surfaces is over and above the increase in surface area due to curvature since an increase in the polymer signal is also accompanied by an increase in substrate signal. The main advantage of SIMS over XPS is that SIMS utilizes the PS signal directly rather than the integrated carbon signal from XPS, which may have small but finite contributions from carbon contaminants. We estimate that a typical error in the measurement of adsorbed amounts from XPS is around ±5%, based on earlier studies in our group. Additionally, there is a ±5% spot-to-spot variation. A maximum error bar of ±30% has been uniformly assigned to all these measurements.

Results

XPS was used to determine the absolute amounts of the polymer adsorbed on smooth Al films. The thickness of the adsorbed film was calculated by assuming an exponential dependence of the photoelectron escape probability with depth as proposed by Fadley[42] et al. For a carbonaceous film on top of an Al substrate, the total integrated Al intensity should vary as

$$\ln\left[\frac{Al_{2p}(\theta)}{Al_{2p}(90°)}\right] = -\frac{\tau}{\lambda}\left[\frac{1}{\sin\theta} - 1\right] \quad (4)$$

where τ is the thickness of the film, λ is the mean free path of the Al_{2p} electrons in the film, and θ is the takeoff angle. This formulation was used earlier by Parsonage[13] et al. for calculating adsorbed amounts of poly(2-vinylpyridine)–polystyrene (PVP–PS) diblock copolymers. They reported a mean free path of 15 Å for the Si_{2p} electrons, which we use in our calculations to determine the thickness of the adsorbed layers. Our conclusions drawn on the relative adsorbed amounts of polymer do not depend on the accuracy of this number. Thickness of the adsorbed layers for the different molecular weights has been tabulated in Table 1. The adsorbed amounts have been determined assuming a bulk density of 1.03 g/cm^3 in the dried, adsorbed films. Surface density has been calculated using the relation $\sigma = sN_{Av}/M$, where s is the adsorbed amount in g/cm^2, M is the molecular weight, and N_{Av} is Avogadro's number. The overlap density corresponds to the condition when adjacent chains just overlap and can be calculated as

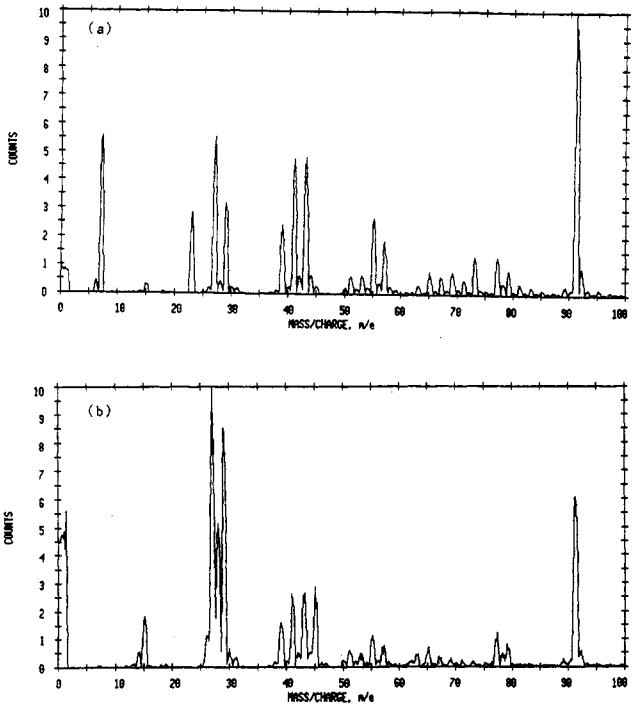

Figure 6. SIMS spectra from M_w = 5700 polystyrene adsorbed on (a) a smooth aluminum surface (scale factor = 4.736 kcounts/s) and (b) a rough surface (40-Å bead size) (scale factor = 0.791 kcounts/s).

$$\sigma_{ol} = 1/(\pi R_{PS}^2) \quad (5)$$

where R_{PS} is the radius of gyration of the PS chains. The radius of gyration for PS chains in toluene is given by Higo[43] et al. and can be calculated as

$$R_{PS} = aN^\nu, \quad a = 1.86 \text{ Å}, \quad \nu = 0.595 \quad (6)$$

where a and N represent the segment length and the degree of polymerization, respectively. In all the cases the measured surface density (σ) is higher than the overlap surface density (σ_{ol}), suggesting that the osmotic interactions in the crowded chains are sufficient to stretch the chains on flat surfaces.

We first discuss adsorption on surfaces synthesized from the 40-Å beads. Figure 6a shows the SIMS spectrum for M_w = 5700 polymer adsorbed on a flat aluminum surface. This can be compared to the corresponding spectrum for the rough surface (40 Å) shown in Figure 6b, which clearly shows a decreased $PS^+(91)$ signal compared to the Al^+-(27) and $AlH^+(28)$ signals from the smooth surface. A significant reduction in the $PS^+(91)$ peak as compared to the $Al^+(27)$ and $AlH^+(28)$ peaks was observed for all the molecular weights. Reductions in the adsorbed amounts were even higher for the other molecular weights. Possible causes for decreased adsorption could be (a) chemical modification of the surface, (b) influence of surface roughness on the recorded spectrum, or (c) surface geometry induced steric hindrance reducing the total amount of polymer adsorbed (Figure 13).

We have attempted to test these possibilities experimentally. The negative secondary ion spectrum on a rough blank substrate shows the same concentration of the hydroxyl ions as a blank flat surface. This rules out chemical differences in surface properties between rough and smooth surfaces as the cause of reduced adsorption since the imine–hydroxyl group interaction is the likely mechanism of grafting. To further eliminate the possibility of chemical modification, a PVP–PS (PVP(15K)–PS-(152K)[13] diblock copolymer was adsorbed from a ~78 μg/mL solution in toluene on these surfaces. Again a decrease in adsorption was observed on the rough surface. This rules out the possibility of chemical modification as this diblock is not chemisorbed.

The main influence of the surface roughness would be to shadow certain areas, preventing collection of ions from these spots. Such effects cannot explain the reduction in the ratio of the polymer signal as compared to the aluminum signal as shadowing would tend to reduce the respective intensities of both signals. It is very important to reiterate the importance of model texture here. In contrast to a randomly rough surface, where the shadowing effects would be random, in this case irrespective of the bead size it would be the same fraction of area which would be shadowed at one angle for all bead sizes. Although the ion yields change as a function of takeoff angle, the overall signal is being integrated over the same range of takeoff angles for different bead sizes. Moreover, the signal is averaged over a large number of beads. It is important to note that the results presented in this paper are with reference to the fraction of the total area from where the ions are collected.

If the reduced adsorption was due to the surface geometry induced steric hindrance, then smoothening the surface should increase adsorption. To check this possibility, in one case (~800-Å bead size) the surface was coated with a thick layer of Al (~500 Å) to flatten the surface. An increase in the adsorbed amounts was observed, confirming the hypothesis that the surface topography was indeed hindering adsorption. A further test of this hypothesis is that the adsorbed amounts are expected to increase with bead size. Larger beads were synthesized and increased adsorption was observed for all molecular weights. This observation basically implies nonuniform adsorption, i.e., higher adsorption on the bumps as compared to the valleys. It is this noncontinuous coverage which results in an increased Al signal and therefore a reduced R_{SIMS}.

Having established the cause of reduced adsorption, we now discuss more general results for large bead sizes and different molecular weights. Five different bead sizes were used for the measurement: 40, 800, 2000, 4000, and 6000 Å in diameter. In all cases, a roughness of 5 Å was arbitrarily assigned as the smooth surface random roughness, where the ratio (R_{SIMS}) was taken to be one. Figure 7 shows the plot of measured R_{SIMS} vs bead size for the three different molecular weights. The smallest molecular weight polymer (Figure 7a) shows reduced adsorption followed by enhancement and then drop back to the smooth surface ratio of one. The decrease to the smooth surface value is consistent with the large bead size limit of R_{SIMS} as discussed earlier. The enhancement in the adsorbed amount over and above the increase in the surface area is most significant. This increase confirms the predictions of enhanced adsorption[32] due to the reduced stretching energy of the chains on curved surfaces. It must, however, be cautioned that there is no one-to-one correspondence between R_{SIMS} and the actual ratio of the adsorbed amounts. The actual ratio of the adsorbed amounts would be a square root[44] or a lower power of this experimental ratio.

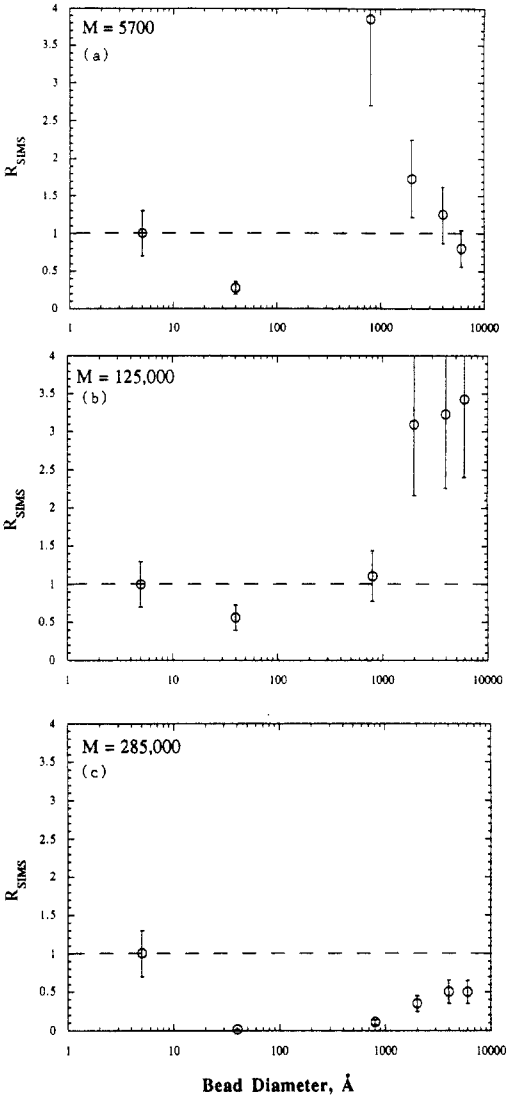

Figure 7. R_{SIMS} as a function of the bead size for the three polymers: (a) M_w = 5700; (b) M_w = 125000; (c) M_w = 285000. Points over the dashed line correspond to enhancement in adsorption, while values below the line indicate a decrease in adsorption as compared to the flat surface.

The next higher molecular weight (125000) also behaves similarly, showing regimes of decrease and increase in adsorption. A fall back to the smooth surface values was, however, not observed in the bead sizes studied. Relatively monodisperse larger size silica dispersions could not be synthesized due to problems of agglomeration of silica particles. No enhancement over the smooth surface values was observed for the highest molecular weight (285000). The adsorbed amounts, however, did increase from negligible amounts at very small bead sizes to close to the smooth surface ratio of unity for the 6000-Å bead size.

Static SIMS has been used as the primary technique for characterizing the adsorbed amount on rough surfaces. The ratio as measured from SIMS (R_{SIMS}) is compared with that from XPS (R_{XPS}) in Figure 8. It can be seen that the two values are positively correlated, demonstrating the consistency between the two techniques.

Discussion

These experiments demonstrate that the amount of end-adsorbed polymer per unit exposed area on a rough surface

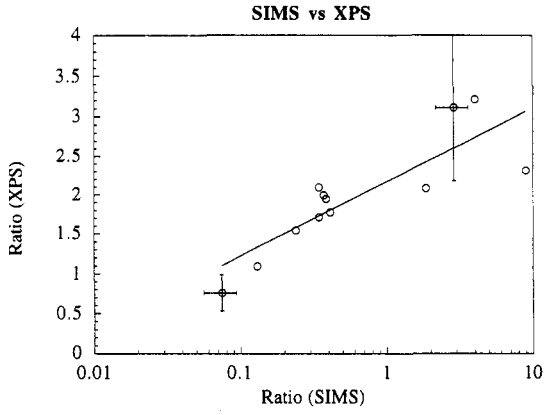

Figure 8. Relation between the ratio of the PS(91) peak to the $Al^+(27)$ and $AlH^+(28)$ peaks as measured from SIMS compared to the integrated C_{1s} intensity over the integrated Al_{2p} counts measured from XPS. The two ratios are positively correlated, indicating the consistency between the two techniques for determining the general trends in adsorption.

Table 2

PS MW	N	L (Å)	R_{PS} (Å)
5700	55	21.99	20.18
125000	1202	177.44	126.5
285000	2740	293.64	206.5

is a complex function of the surface roughness (defined by the size of the beads) and the length of the polymer chain. A region of reduced adsorption is followed by a region of enhanced adsorption with increase of bead diameter. As the molecular weight of the polymer is increased, these regimes shift to higher bead sizes. In this section we discuss ideas relating to the functional dependence of the adsorbed amounts on the bead size and the length of the polymer chain. A crude, qualitative comparison with a current theoretical model of adsorption on a single bump (on a flat surface) is possible.

To test for universal behavior for the various cases, we have tried reducing the data in terms of possible scaling behavior. Three evident choices of characteristic macromolecular dimensions for scaling the bead size by the polymer size are the radius of gyration, the layer thickness, and the contour length. In the case of end-grafted polymers, scaling by the layer thickness and the radius of gyration is relevant. Since the surface density is in the neighborhood of the overlap density (Table 1), the chains are not strongly stretched and the scaling by R_g or layer thickness is expected to be similar. In the absence of any way to measure the layer thickness, we have estimated this length by calculating the stretched chain length using the formulas proposed by Ligoure[32] et al.

For $L/\rho \gg 1$, i.e., for very extended grafted layers, the stretched chain length[32] is given by

$$L_d \simeq \rho\alpha_d^{-\alpha_d}\left(\frac{Na}{\rho}\sigma^{(D-1)/2}\right)^{\alpha_d} \tag{7}$$

where $D \simeq 5/3$ is the fractal dimension of the excluded volume chains, α_d is the characteristic exponent which equals 1 for flat surfaces ($d = 1$), $3/4$ for cylindrical surfaces ($d = 2$), and $3/5$ for spherical surfaces ($d = 3$). In our case the chains are not strongly stretched. A more general expression for the stretched chain length has been derived from the blob model using the formalism outlined by Ligoure and Leibler without using the approximation L/ρ

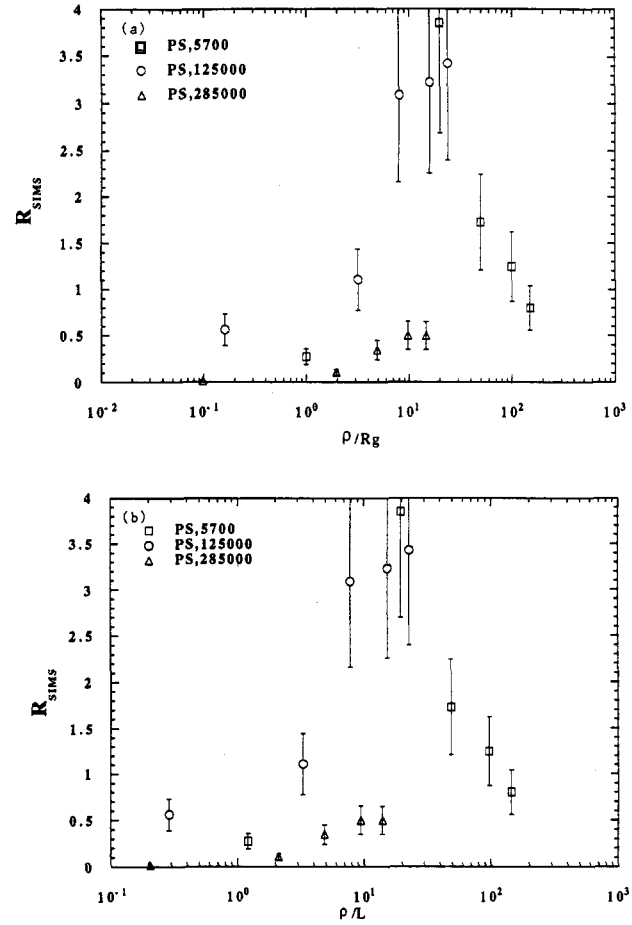

Figure 9. (a) Coil scaling: R_{SIMS} vs bead size scaled with the radius of gyration. (b) Linear scaling: R_{SIMS} vs bead size scaled with the stretched chain length. Both the stretched chain length and the radius of gyration scale similarly, indicating that the chains are not greatly stretched. The scaled profile shows regions of reduction followed by enhancement and a decrease back to the smooth surface ratio of one.

$\gg 1$. Stretched chain length for the case of adsorption on spherical bumps is then given by

$$L = \rho\left[\left(1 + \frac{5N}{3}\sigma^{1/3}\frac{a}{\rho}\right)^{3/5} - 1\right] \tag{8}$$

The radius of gyration is calculated using eq 6. Stretched chain lengths for grafting on the flat surface are listed in Table 2.

Figure 9 shows the scaling for the three molecular weights when the bead size is scaled with respect to the radius of gyration (R_g) (Figure 9a) or the stretched chain length (L) (Figure 9b). Both R_g and L scale the three profiles similarly, consistent with the idea that the chains are not strongly stretched. The reduced profile is characterized by three regimes as described below.

Regime I: Reduction (ρ/R_g or $\rho/L < 1$). This regime occurs when ρ/R_g or $\rho/L < 1$, i.e., when less than one coil is adsorbed on one bead ($\rho \approx R_g$) as sketched in Figure 10a. The low value of R_{SIMS} results from the combined effect of an increased substrate signal ($\propto 2\pi R_g^2$) from the hemispherical bump as compared to that for the corresponding flat surface ($\propto \pi R_g^2$), accompanied by a decreased adsorption in the valleys between beads. The decrease in adsorption is interpreted in terms of reduction in the area available for adsorption by steric hindrance. Coils adsorbed on the bumps impede adsorption in the valleys of the surface, resulting in a decreased coverage.

Another possible cause for the reduced adsorption can be the influence of capillarity in preventing wetting of the

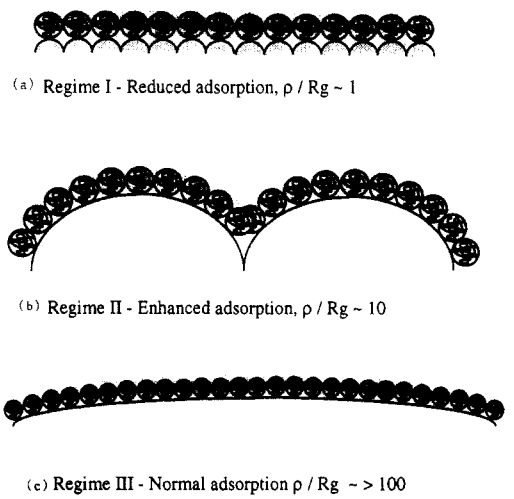

Figure 10. (a) Regime I: Steric hindrance induced reduction in adsorption when one coil is adsorbed on one bead. (b) Regime II: Enhancement when approximately ten coils adsorb on one bead. (c) Regime III: Smooth surface behavior for high radius of curvature when the surface looks flat.

solution in the crevices. However, on comparing the data for the 800-Å beads (Figure 7) for the three molecular weights, it can be clearly seen that while there is an enhancement in the 5700 MW adsorption, the highest molecular weight polymer continues to adsorb minimally. This clearly eliminates capillarity being a cause for the reduced adsorption since the smallest molecular weight polymer does adsorb significantly, implying sufficient wetting of the surface by the solution.

Regime II: Enhancement (ρ/R_g or $\rho/L \approx 10$). Surface curvature induced enhancement in the surface density is the most notable observation in this work. As explained earlier, this increase is over and above the increase due to the physical surface area available for adsorption. This regime of increased adsorption can be visualized to occur when approximately ten coils ($\rho/R_g \approx 10$) adsorb on one bead as illustrated in Figure 10b. An increase in surface density can be explained by a favorable decrease in the stretching free energy for the same surface coverage as compared to a flat surface. Although definite enhancements in adsorption were observed for the two lower molecular weights, no increase over the smooth surface ratio of one was recorded for the highest molecular weight. A possible explanation for this is taken up later in the discussion.

The stretched chain lengths have been calculated using the overlap surface density as it is not possible to quantitatively determine the surface density for each bead size in situ. In this region of enhancement the actual stretched chain lengths will be larger than those estimated using the overlap surface density. This implies that in reality the ratio ρ/L where the adsorption maximizes is smaller than that computed through this estimation of the stretched chain length.

It is conceivable that the polymer might adsorb nonuniformly on some of the textured surfaces. Noncontinuity of the film would imply an increased substrate signal and therefore a reduced R_{SIMS}. While this nonuniformity is possibly the cause of the reduced adsorption as discussed above, it cannot explain the enhancement we observe.

Regime III: Normal (ρ/R_g or $\rho/L > 100$). As the bead size is increased further, R_{SIMS} falls back to the smooth surface value of one. This implies that at high curvatures the surface is essentially flat as shown in Figure 10c. Flat

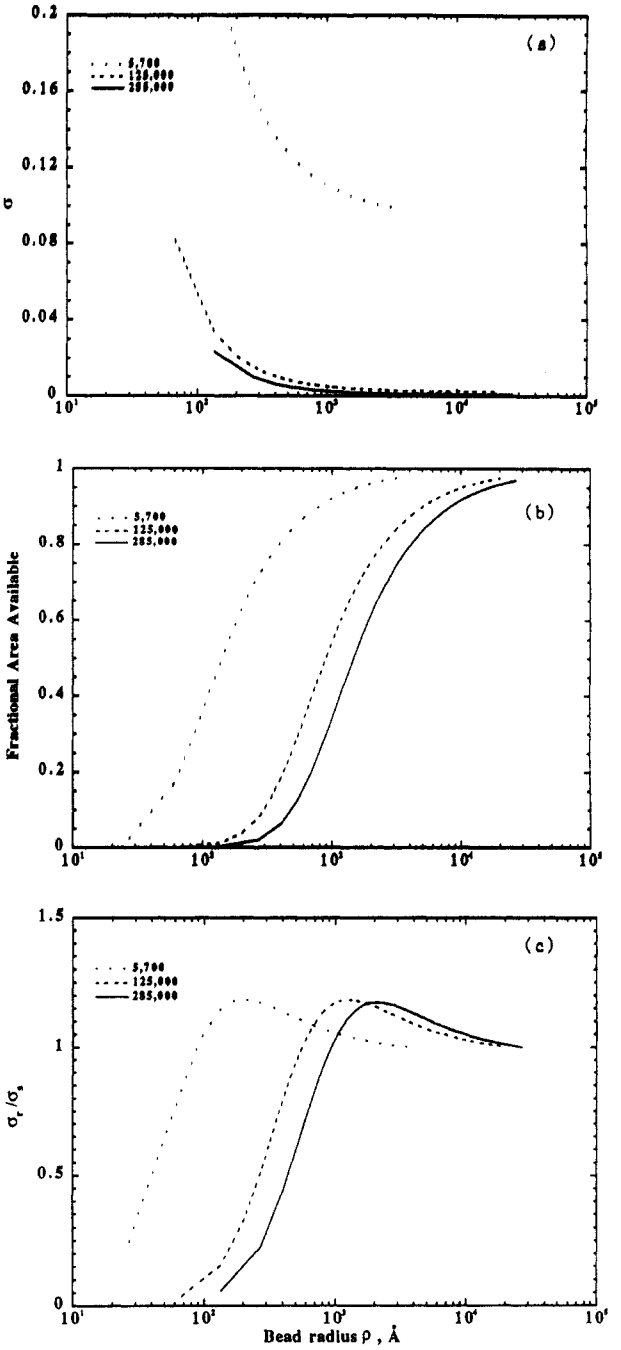

Figure 11. (a) Enhancement in adsorption as predicted from the calculations of Ligoure and Leibler[32] as a function of bead size for the three different molecular weights. These calculations are for adsorption on a single spherical bump on a flat surface. (b) Fractional area available for adsorption as a function of bead size for the three polymer chain lengths. (c) A crude convolution of the increase in adsorption and the fractional area available showing regions of decrease in adsorption followed by enhancement and then fall back to the smooth surface ratio. The maximum in adsorption shifts to higher bead sizes with increase in polymer chain length.

surface behavior was observed when the coil radius of gyration or the stretched chain length is <1% of the radius of curvature of the surface.

The intermediate region of increase in adsorption is consistent with predictions of enhancement by Ligoure and Leibler for adsorption on an isolated bead. Their expressions have been used to calculate the variation in surface density as a function of bump size for the three different molecular weights as shown in Figure 11a. The calculated surface density[32] increases as the bead size decreases.

Physically, in the limit of zero bead size, the topography approaches that for a smooth surface and in this limit the ratio of surface coverage should fall back to the smooth surface value of one. This feature is not recovered from these calculations. Moreover, since this theory has been developed for the case of adsorption on a single bump on a flat surface, the influence of molecules adsorbed on adjacent beads has not been considered. The primary influence of adsorption on neighboring bumps would be to sterically hinder adsorption in the valleys, thereby reducing the effective area available for adsorption. In a crude attempt to explain our results, we have accounted for this steric influence by assuming that when chains on adjacent bumps overlap more than two-thirds (arbitrary value taken) their extended length in solution, adsorption in the shadowed area under the chains is prevented, as illustrated by the darkened areas in Figure 13. Figure 11b shows the variation in the fractional area available for adsorption as a function of bead size for the different molecular weights. This fractional availability of area can be convoluted with the single bump enhancement curves computed above (Figure 11a), and the result is shown in Figure 11c.

In this figure, a region of reduced adsorption is followed by enhancement, which then falls back to the smooth surface values, consistent with the experimental results. With increase of molecular weight, the enhancement occurs at higher ρ/L values. It is possible that we did not observe any enhancement for the highest molecular weight because the largest bead size studied was not large enough to result in an enhancement of adsorption. Larger bead sizes could not be synthesized because of the limitations in getting a relatively monodisperse distribution at large particle sizes. It must be mentioned that these curves have been calculated for surface densities much greater than the overlap surface densities. The main intention of these calculations is to illustrate the qualitative similarities and not make any quantitative comparisons. Figure 12a shows that if the bead size is scaled with respect to the radius of gyration, then these three curves collapse onto one single curve, with the maximum around $\rho/R_g \sim 10$. This result is consistent with the experiments, but it must be noted that this comparison is not rigorous by any means. Scaling by L as shown in Figure 12b also results in a similar collapse, but the maximum now occurs around $\rho/L \sim 1$, which is not consistent with experiments possibly because the chains are not strongly stretched in the actual experimental situation.

In summary, these results demonstrate that the surface roughness can have significant influence on adsorption and grafting. These model surfaces provide the opportunity to test the various theoretical predictions, which can then be extended to the case of randomly rough surfaces. Fractal dimension might be used to characterize the randomness of the surfaces in such cases. One significant implication of these experiments is that when a polydisperse end-functionalized polymer is adsorbed on a rough surface, the local radius of curvature might favor adsorption of different molecular weights. Extending it to the case of adsorption on colloidal particles, adsorption of polymers with stretched chain lengths comparable to the radius of these particles will be favored.

One of our significant achievements has been the synthesis of model rough surfaces. These surfaces can also be used in several other studies requiring controlled surface modulations. As an example these model surfaces provide ideal substrates for quantifying off-specular reflection. Our preliminary studies show dips in the specular reflectivity in the critical region due to off-specular scattering. The position of this minimum shifts with bead size. It will be interesting to test some of the current theories on off-specular scattering to explain these shifts and relate the off-specular scattering to the surface fluctuations.[45]

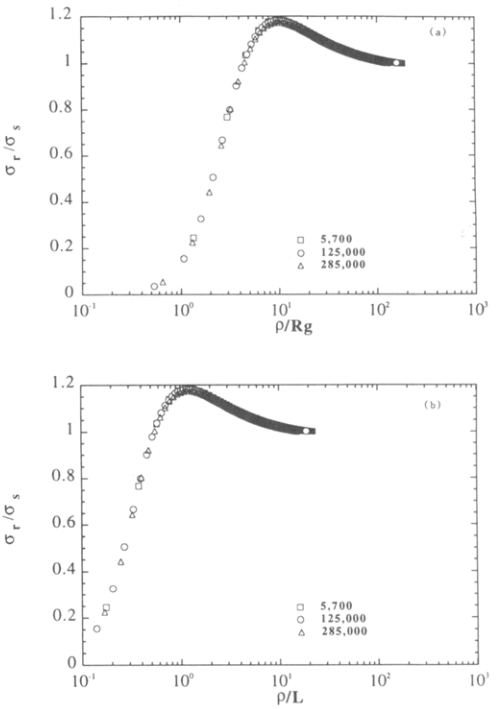

Figure 12. (a) The three calculated curves collapse onto one curve when the bead size is scaled with the radius of gyration. The maximum occurs around $\rho/R_g \sim 10$, consistent with the experimental results. (b) Collapse of the three curves when the bead size is scaled with the stretched chain length. The maximum now occurs around $\rho/L \sim 1$, in contrast to the experimental result of $\rho/L \sim 10$. One possible reason for this discrepancy is that under the experimental conditions the chains are not strongly stretched.

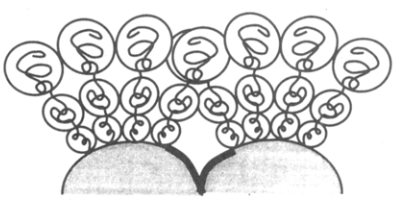

Figure 13. Grafting of chains on the bumps results in overlap over the valleys, preventing adsorption in the shaded areas. The fractional area unavailable for adsorption has been calculated by assuming that no adsorption occurs in regions where chains overlap more than two-thirds of their stretched chain length.

Conclusions

We report the successful synthesis of model rough surfaces, which can be used for a controlled study of the influence of surface fluctuations on adsorption. The surface roughness is defined by the radius of the silica spheres, which can be controlled during the chemical synthesis of the beads. Three regimes have been observed for the adsorption of end-functionalized polymers on these surfaces. For very small bead sizes, or very low ρ/R_g, a steric hindrance induced region of reduced adsorption has been observed. At intermediate sizes the surface density of the polymers on the surface increases over and above the smooth surface value, consistent with the predictions from the blob model. As the bead size is increased further, the surface density falls back to the smooth surface value,

indicating that the surface curvature for this chain size was large enough to treat the surface as being smooth, and any absolute increase in adsorption is simply due to the increase in surface area.

Acknowledgment. We thank Jon V. De Groot, Jr., for help in the synthesis of the silica beads and SEM, Terry Stange for help with AFM on these model surfaces, William Katz and Gary Smith at Evans Central for SIMS, Raul Carreta and Dizhong Liu for XPS, Larry Zazzera for ozone cleaning, Uttandaraman Sundararaj for some initial SEM, and Sushil Satija and Chuck Majkrzak for X-ray reflectometry characterization of the substrates. We also acknowledge useful discussions with Pat Brant, Glenn Fredrickson, M. Muthukumar, Nily Dan, Sunil Dhoot, Ashish Khandpur, and Mohan Sikka. We acknowledge partial support from the Petroleum Research Fund, administered by the American Chemical Society. Partial support for this research was also received from the National Science Foundation (Grant NSF/CTS-9107025, Interfacial Transport and Separations Program [CTS] and Polymers Program [DMR]).

References and Notes

(1) Halperin, A.; Tirrell, M.; Lodge, T. P. *Adv. Polym. Sci.* **1992**, *100*, 31.
(2) Russell, W. B.; Saville, D. A.; Schowalter, W. R. *Colloidal Dispersions*; Cambridge University Press: Cambridge, 1989.
(3) Hench, L. L.; Ulrich, D. R., Eds. *The Science of Ceramic Chemical Processing*; Wiley: New York, 1986.
(4) Alexander, S. *J. Phys.* (*Fr.*) **1976**, *38*, 977.
(5) De Gennes, P.-G. *Macromolecules* **1980**, *13*, 1069.
(6) (a) Milner, S. T.; Witten, T. A.; Cates, M. E. *Macromolecules* **1988**, *21*, 2610. (b) Muthukumar, M.; Ho, Jyh-Shyong *Macromolecules* **1989**, *22*, 965.
(7) Milner, S. T. *Science* **1991**, *251*, 905.
(8) Ligoure, C.; Leibler, L. *J. Phys.* (*Fr.*) **1990**, *51*, 1313.
(9) Marques, C.; Joanny, J. F.; Leibler, L. *Macromolecules* **1988**, *21*, 1051.
(10) Hadziioannou, G.; Patel, S.; Granick, S.; Tirrell, M. *J. Am. Chem. Soc.* **1986**, *108*, 2869.
(11) Tirrell, M.; Patel, S.; Hadziioannou, G. *Proc. Natl. Acad. Sci. U.S.A.* **1987**, *84*, 1725.
(12) Taunton, H. J.; Toprakcioglu, C.; Klein, J. *Macromolecules* **1988**, *21*, 3333.
(13) Parsonage, E.; Tirrell, M.; Watanabe, H.; Nuzzo, R. G. *Macromolecules* **1991**, *24*, 1987.
(14) Tirrell, M.; Parsonage, E.; Watanabe, H.; Dhoot, S. *Polym. J.* **1991**, *23* (5), 641.
(15) Daoud, M.; Cotton, J. P. *J. Phys.* (*Fr.*) **1982**, *43*, 531.
(16) Birshtein, T. M.; Zhulina, E. B. *Polymer* **1984**, *25*, 1453.
(17) Birshtein, T. M.; Zhulina, E. B.; Khokhlov, A. R.; Yurasova, T. A. *J. Polym. Sci. USSR* (*Engl. Transl.*) **1987**, *29*, 1293.
(18) Birshtein, T. M.; Borisov, O. *V. Polymer* **1991**, *32*, 923.
(19) Cates, M. E.; Safran, S. A.; Witten, J. A. *J. Chem. Phys.* **1987**, *87*, 1824.
(20) Witten, T. A.; Pincus, P. A. *Macromolecules* **1986**, *19*, 2509.
(21) Milner, S.; Witten, T. A. *J. Phys.* (*Fr.*) **1988**, *49*, 1951.
(22) Grest, G. S.; Kremer, K. *Phys. Rev. A* **1986**, *33*, 3628.
(23) Grest, G. S.; Kremer, K.; Witten, T. A. *Macromolecules* **1987**, *20*, 1376.
(24) Murat, M.; Grest, G. S. *Macromolecules* **1991**, *24*, 704.
(25) Ball, R. C.; Marko, J. F.; Milner, S. T.; Witten, T. A. *Macromolecules* **1991**, *24*, 693.
(26) Dan, N. Ph.D. Thesis, University of Minnesota, 1992.
(27) Auroy, P.; Auvray, L.; Leger, L. *Phys. Rev. Lett.* **1991**, *66*, 719.
(28) Khasat, N.; Pennisi, R.; Hadjichristidis, N.; Fetters, L. J. *Macromolecules* **1988**, *21*, 1100.
(29) Kawaguchi, M.; Anada, S.; Nishikawa, K.; Kurata, N. *Macromolecules* **1992**, *25*, 1588.
(30) Hone, D.; Ji, H.; Pincus, P. A. *Macromolecules* **1987**, *20*, 2543.
(31) Blunt, M.; Barford, W.; Ball, R. *Macromolecules* **1989**, *22*, 1458.
(32) Ligoure, C.; Leibler, L. *Macromolecules* **1990**, *23*, 5044.
(33) Balazs, A. C.; Huang, K.; Lantman, C. W. *Macromolecules* **1990**, *23*, 4641.
(34) Andelman, D.; Joanny, J. F. *Macromolecules* **1991**, *24*, 6040.
(35) Stöber, W.; Fink, A.; Bohn, E. *J. Colloid Interface Sci.* **1968**, *26*, 62.
(36) Bogush, G. H.; Tracy, M. A.; Zukoski, C. F. *J. Noncryst. Solids* **1988**, *104*, 95.
(37) (a) Kitahara, S.; Watanabe, H.; Kawanaka, T.; Furusawa, K. *Kobunshi Ronbunshu* **1992**, *49*, 921. (b) Furusawa, K.; Ogawa, T.; Itabashi, T.; Kitahara, S.; Watanabe, H. *Kobunshi Ronbunshu* **1992**, *49*, 915.
(38) Katz, W.; Newman, J. G. *Mater. Res. Soc. Bull.* **1987**, *12* (6), 40.
(39) Briggs, D. *Polymer* **1984**, *25*, 1379.
(40) (a) Hearn, M. J.; Briggs, D.; Yoon, S. C.; Ratner, B. D. *Surf. Interface Anal.* **1987**, *10*, 384. (b) Smith, G., personal communication.
(41) Newman, J. G.; Viswanathan, K. V. *J. Vac. Sci. Technol. A* **1990**, *8* (3), 2388.
(42) Fadley, C. S.; Baird, R. J.; Siekhaus, W.; Novakov, T.; Bergstorm, S. A. L. *J. Electron Spectrosc. Relat. Phenom.* **1974**, *4*, 93.
(43) Higo, Y.; Ueno, N.; Noda, I. *Polym. J.* **1983**, *15*, 367.
(44) The ratio of the polymer to the substrate signal is being measured through R_{SIMS}. For a fixed penetration depth (D), the ratio R_{SIMS} for a polymer layer of thickness T would be $T/(D - T)$. An increase in the polymer signal results in a corresponding decrease in the substrate signal (therefore the square dependence), amplifying the effect of the small increase in adsorption when measured in the form of this ratio. It is the sensitivity of this ratio to the adsorbed amounts which has enabled us to record subtle changes in adsorbed amounts.
(45) Karim, A.; Singh, N.; Tirrell, M.; Bates, F. S.; Satija, S. K.; Majkrzak, C. F., unpublished results.